Journal of Power Sources 184 (2008) 532–537

Contents lists available at ScienceDirect

Journal of Power Sources

journal homepage: www.elsevier.com/locate/jpowsour

Short communication

A new process of preparing composite microstructure anode for lithium ion batteries

Hai-peng Zhao[a,b,*], Chang-yin Jiang[a], Xiang-ming He[a], Jian-guo Ren[a]

[a] Institute of Nuclear & New Energy Technology, Tsinghua University, Beijing 100084, PR China
[b] Pingdingshan Institute of Technology, Henan 467000, PR China

ARTICLE INFO

Article history:
Received 18 December 2007
Received in revised form 23 January 2008
Accepted 24 February 2008
Available online 29 February 2008

Keywords:
Lithium ion batteries
Electro-deposition
SnSb alloy
Composite anode
Cycle performance

ABSTRACT

A composite material anode for lithium ion batteries (LIB) consisted of electrodeposited Sn–Sb alloy dispersing in a conductive micro-porous carbon membrane coated on Cu current collector was investigated. The composite material was obtained by directly electrodepositing Sn–Sb alloy on the micro-porous membrane electrode via micro-pores in it, which was prepared by casting a polyacrylonitrile (PAN) solution containing polyethylene glycol (PEG) on a copper foil and then immersing the copper foil into de-ionized water to perform phase inversion, following by heat-treatment. SEM examinations showed that the composite material consisted of isolated pillar-like structure SnSb electrodeposited on Cu current collector dispersing in a conductive micro-porous carbon membrane deriving from pyrolysis of PAN. Constant current charge and discharge tests using the composite anode showed stable coulombic efficiency and desirable cyclability. The reversible discharging capacity was 339.5 mAh g^{-1} after 50 cycles, corresponding to 78.6% of the discharge capacity retention.

1. Introduction

Lithium ion batteries are currently the best portable energy devices for the consumer electronics. Carbon materials (hard carbon, soft carbon, graphite, etc.) are commercially used as the anode material of lithium ion battery. In view of the fact that the theoretical capacity of carbon material is only 372 mAh g^{-1}, to get higher energy and power densities, a significant attention has been paid to investigation of many alloy materials. These alloy materials, such as Sn-based alloy, Si-based alloy, Sb-based alloy, etc., used as anodes for lithium ion batteries may exhibit larger specific gravimetric and volumetric capacities [1–4]. However, they have a common drawback, which is the pulverization of alloy caused by its volume expansion/shrinkage during the charge/discharge cycles of lithium ion batteries associated with the reversible reaction of Li. Such morphological changes results in severe cracking of electrode with loss of electrical contact between inter-particles, and particle and the current collector, resulting in poor charge/discharge cycling characteristics. Therefore, it is necessary to relieve such morphological changes to achieve satisfactory cycling performance. Many research findings have shown that abovementioned problems can be resolved to some extent by using nanocrystalline [5–7], porous materials [8] and by using multi-component instead of single-component materials like binary phases Cu_6Sn_5 [9–11], which due to their complex reaction mechanism help to relieve mechanical strain during charge and discharge of the material. However, macroscopical alloy particles will still suffer from pulverizing risk in long-term cycles as a result of the rapid loss of the reversible capacity. Although the introduction of nano-sized materials can strongly affect reversible capacity, it confronts still some unsolved problems such as the reaggregation of nanometer alloy particles during cycling. Nevertheless, when superfine alloy particles are dispersed in suitable supporting medium such as amorphous carbon network, the resulting composite materials should be very effective in maintaining dimensional integrity during cycling [12–14], where the carbon network acts as a barrier to prevent the aggregation between the nanometer alloy particles, and provides a void space where the particles experience a volume change.

Polyacylonitrile (PAN) is a linear and insulated macromolecule at room temperature. Thermally treated polymer of PAN shows a rich evolution of structural and electric properties, the chains undergoing cyclization to form a conjugated-chain chemical structure, resulting in electrical conductivity. Thus, PAN becomes conjugated conducting polymer by low temperature pyrolysis [15].

In the other hand, PAN is a very processable polymer, which can be dissolved in DMF or DMSO to form casting solution. After the casting solution cast on a glass plate was properly treated by phase inversion process, a microporous PAN membrane can be obtained. In the present study, we attempted to prepare composite material by electrodepositing Sn–Sb alloy on a template-like microporous

* Corresponding author at: Institute of Nuclear & New Energy Technology, Tsinghua University, Beijing 100084, PR China. Tel.: +86 10 89796036; fax: +86 10 89796031.
E-mail address: zhaohp05@mails.tsinghua.edu.cn (H.-p. Zhao).

0378-7753/$ – see front matter © 2008 Elsevier B.V. All rights reserved.
doi:10.1016/j.jpowsour.2008.02.064

Table 1
Bath composition and operating conditions for preparing electrode

Materials	Concentration ($g L^{-1}$)
$SnCl_2 \cdot 2H_2O$	30
$SbCl_3$	2
$K_4P_2O_7 \cdot 10H_2O$	130
Tartaric acid	7
Gelatin	0.3
Temperature	44–50
Current density ($mA cm^{-2}$)	2
pH	7.5–8.2
No stirring	

membrane electrode, which was prepared by casting PAN solution on a copper foil following phase inversion in a non-solvent water, and then heat-treatment. The composite material with dispersed Sn–Sb alloy in conducting carbon network showed better cycle performance.

2. Experimental

The polymer PAN (its weight-average (M_w) values: about 1.5×10^5 g mol^{-1}) used in this study was synthesized by suspension polymerization in our laboratory. A homogenous casting solution of polyacrylonitrile (PAN) was obtained under the mechanical agitation by dissolving 1 g of PAN in 20 mL of dimethylformamide (DMF) solution in which about 5 mL of polyethylene glycol (PEG) was contained. After leaving still for certain time, the resulting viscous solution was cast by a home-made blade with a about 30 μm gap onto a rimmed Cu foil (thickness: 30–40 μm), which was treated in corrosive hydrochloric acid solution in advance. After exposed to air atmosphere at room temperature for appropriate time, the Cu foil was immediately immersed in a de-ionized water bath (a non-solvent coagulating bath) for at least 4 h to perform phase inversion. After the exchange of DMF and water by phase inversion, a substantial number of micro-pores were formed in the film coated on the Cu foil. The resultant was washed, rinsed and dried at 80 °C under vacuum for 24 h, successively. In the end, a white, opaque membrane was firm adhered to the Cu foil and thus a micro-porous membrane electrode was obtained.

The composite anode material for LIB was prepared by electrodepositing Sn–Sb alloy into the as-obtained micro-porous membrane electrode through membrane pores in it, where the membrane electrode was used as working electrode and a pure Sn plate as counter electrode. Compositions and operating conditions of a pH 8.5 electroplating bath are shown in Table 1. All electrodeposition runs were carried out at 44–50 °C without agitation. After electro-deposition, heat-treatment and preparation of tested anode foil were done as follows: the as-electrodeposited composite electrode foil as well as unelectrodeposited micro-porous membrane electrode were cut into circular sheets of diameter 1 cm and then put them into a quartz tube furnace. The heat-treatment was performed under the protection of nitrogen gas at appropriate temperature. Different temperature and time of heat-treatment were tried to optimize parameter of heat-treatment. Based on electrochemical performance and conduction of pyrolytic PAN, the proper temperature for heat-treatment of the electrode foils was carried out in the range of 250–350 °C under the atmosphere of N_2 for 14 h.

Electrochemical tests were performed on 2032-type coin cells with lithium metal (0.5 mm thick foil) as a counter electrode. The electrolytes used were 1 M $LiPF_6$ EC + DEC + DMC (1:1:1, v/v/v). The separator of cell was Celguard 2400. The cell assembly was performed in a glove box filled with argon gas (less than 2 ppm of water). The charge–discharge cycling of the coin cell was galvanostatically performed at a current density of 0.25 mA cm^{-2} with cut-off voltages of 0.02–2.0 V at room temperature. Cycle test was conducted using Land Battery Test System made by Wuhan Land Electronic Co. Ltd. In this study, the charging and discharging processes represent Li-de-insertion and Li-insertion processes, respectively. The amount of active materials in sample was calculated as follows.

Amount of active materials = total weight of anode sheet − weight of corresponding copper current collector or copper substrate, where corresponding copper current collector or copper substrate was the same treatment processes as that of the composite anode foil or unelectrodeposited micro-porous membrane electrode sheet.

Please note, herein, that PAN-pyrolyzed carbon was still regarded as active material in the composite electrode though its reversible capacity is very low. (The amount of Sn–Sb alloy in sample was calculated as follows: amount of active materials = total weight of anode sheet − weight of corresponding heat-treated unelectrodeposited micro-porous membrane electrode sheet.)

Crystal structures of samples were characterized by X-ray diffractometer (XRD, D/max-RB) using Cu Kα radiation. For the cross-section observation, the micro-porous membrane electrode foils were inlaid in an epoxy resin. The epoxy resin was cut, ground and dried to obtain cross-section of them. Before passing through SEM, the cross-section samples of the composite material had to go through the carbon coating process. After that, the samples were imaged and photographed by employing a scanning electron microscope (SEM: JSM6301, Hitachi, Ltd.) with energy dispersion X-ray spectroscopy (EDXS, ATW Link Isis300) with potentials of 15 kV in achieving magnification ranging from 100× to 50,000× to examine the membrane cross-section and the surface. The differential discharging capacity profiles during 1st, 2nd, 10th and 20th for the composite material anode derived from discharge/charge voltage versus capacity profiles of the composite material anode at the constant current density of 0.25 mA cm^{-2} cycled between 0.02 and 2.0 V (vs. Li/Li$^+$).

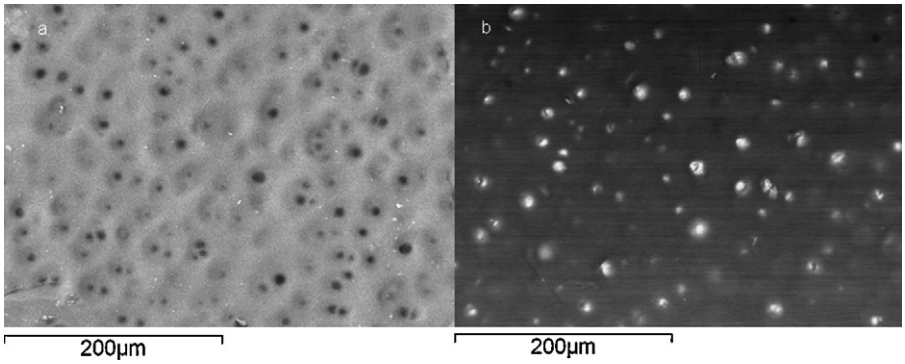

Fig. 1. the electrons back scattered images of surface morphology of microporous membrane electrode before (a) or after (b) electrodepositing.

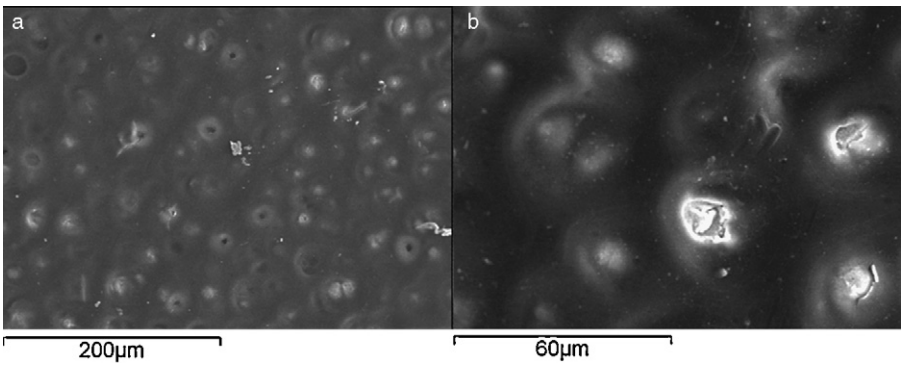

Fig. 2. The secondary electron images of surface morphology of the composite material (a) and its local amplificatory images (b).

3. Results and discussion

Fig. 1 shows the electrons back scattered images of surface morphology of microporous membrane electrode before or after electrodeposition. From Fig. 1a, one can observe that many pores asymmetrically distributed in the surface of the membrane electrode. When the microporous membrane electrode as cathode was put into Sn–Sb alloy plating bath, plating solution went into membrane layer through these pores. While electrodeposition was performing, Sn–Sb alloy first deposited on some places of Cu col-

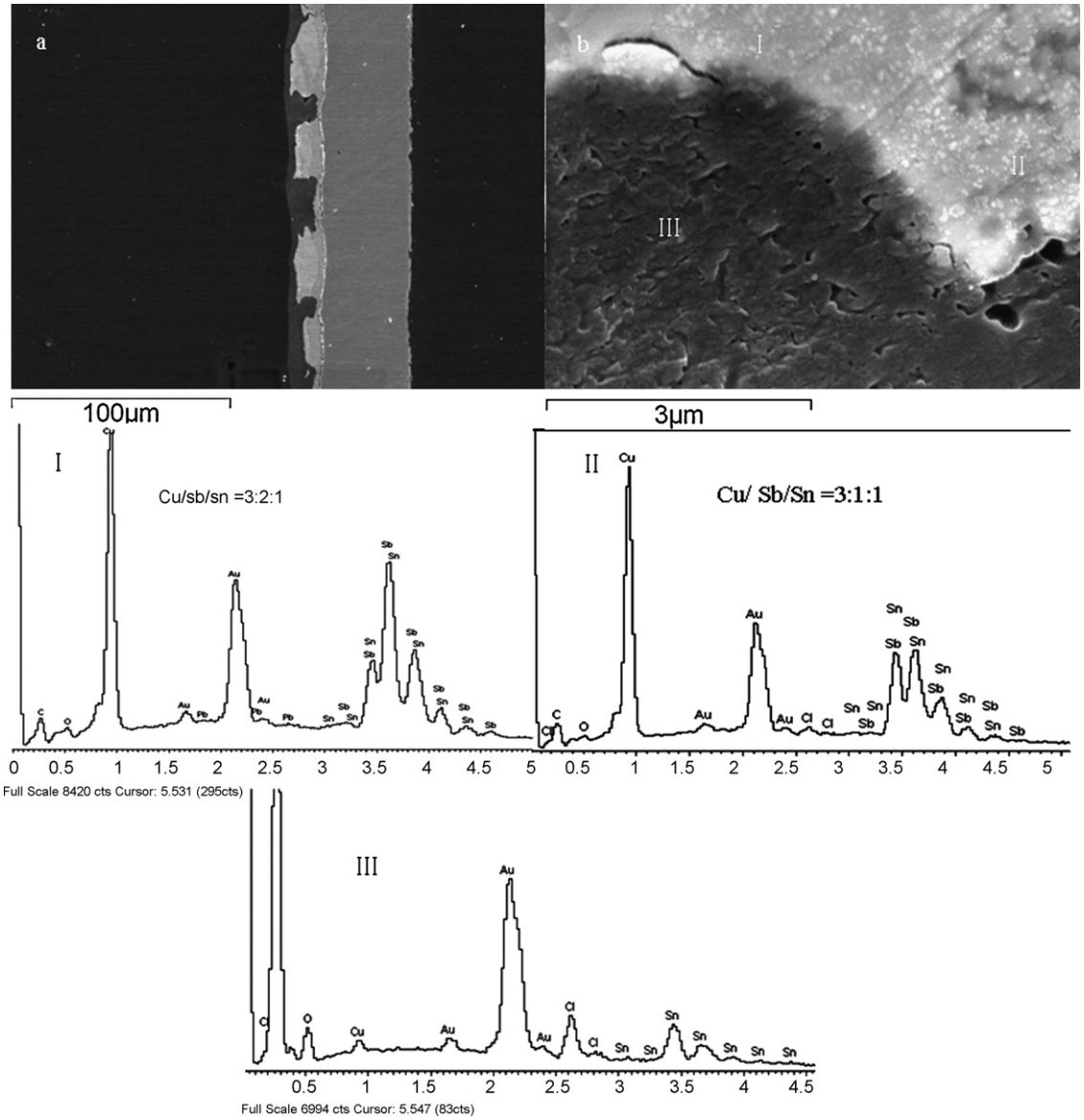

Fig. 3. The cross-section of the composite material (a) and its local amplificatory images (b).

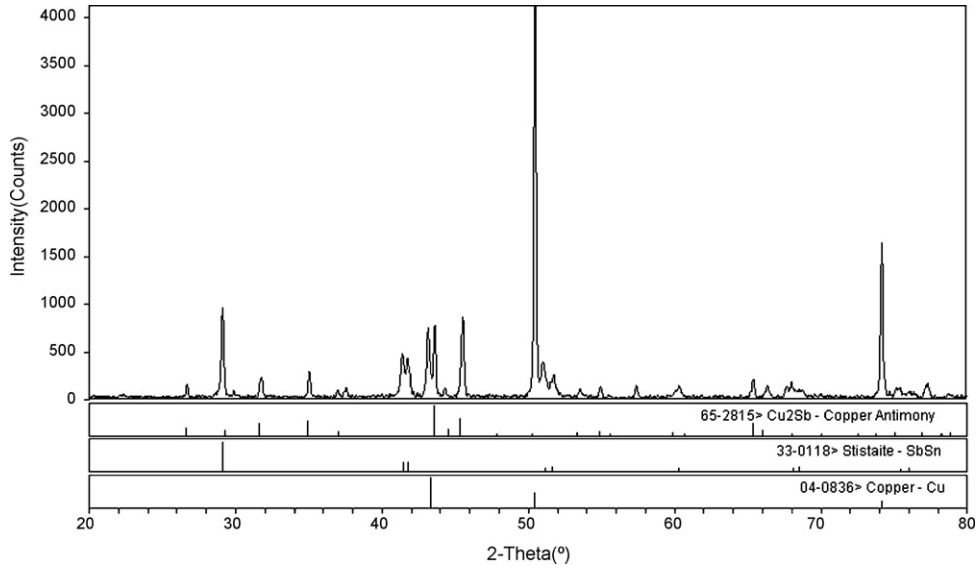

Fig. 4. The XRD patterns of the composite material after heat-treatment at 300 °C.

lector, where these parts exposed to plating solution in membrane layer, and then gradually grew via these membrane pores. As is seen in Fig. 1b, the electro-deposits growing from the membrane pores almost fill in all membrane pores. In the secondary electron images (Fig. 2a) and the local amplificatory secondary electron images (Fig. 2b) of the composite material, it can be noticed that that these electrodeposits do not still come out the membrane surface while only parts of them make surface membrane breach and become exposed. These electrodeposits seems to be ball-like particles and the diameter of about 5–10 μm. However, the cross-section of the composite material shows that the electrodeposits distribute in pillar-like structure not ball-like particles in conductive carbon network pyrolyzed from PAN and approach to membrane surface (Fig. 3a), which is consistent with abovementioned observation. In these isolated pillar-like structure, expansion of these alloys would suffer from less restriction, which was in favor of structural stability of the composite material. This is because there are many pores and channels in amorphous carbon surrounding electrodeposits or interface between electrodeposits and the amorphous carbon (seeing Fig. 3b), which is as a result of ring closure of the nitrile side groups and structural shrinkage of macromolecule PAN as well as release of small-molecule compounds in PAN during annealing. These pores and channels, which should have the same function as voids in plating layers found by Wang et al. [16] and Tamura et al. [17], are quite valuable to accommodate volume change during intercalation and de-intercalation of Li^+ and improve the cycle life of electrode. The EDS analysis indicates that the Cu/Sb/Sn ratio of electrodeposits in the vicinity of Cu substrate is about 3:2:1 (Fig. 3a), which shows that electro-deposition of Sb predominated at the initial stage of electro-deposition. Owing to the excess of Sb, Cu_2Sb would be probably formed with Cu diffusing from Cu substrate during heat-treatment, which would be able to be detected in XRD pattern. In the EDS analysis of electrodeposits far away from Cu substrate, one can observe that Sn/Sb ratio has approached to 1:1 while content of Cu is still high (Fig. 3b), whereas there only is less amount of Cu in the field of amorphous carbon surrounding electrodeposits (Fig. 3c). This indicates that Cu disperses easier in the alloy phase than in amorphous carbon.

Fig. 4 shows the XRD patterns of the composite material after heat-treatment at 300 °C. Based on the XRD pattern, it can be identified that the composite material includes three substances SnSb, Cu_2Sb and Cu, respectively, based on JCPDS no. 33-0118, JCPDS no. 65-2815 and JCPDS no. 04-0836. Herein, from relative strength of Cu peak, we do not still determine whether the reflection peaks of Cu is from the reflection of the Cu current collector or Cu dispersed in the composite material diffusing from the Cu substrate. However, according to information in the EDS analysis, we seem to be able to presume that the diffraction peak of Cu should be from Cu diffusing from Cu substrate during heat-treatment and one part of them forms Cu_2Sb with excess Sb in electrodeposits while the other disperses in the electrodeposits.

Fig. 5 shows the typical charge/discharge curves for the composite material at a constant current density of 0.25 mA cm^{-2} cycled between 0.02 and 2.0 V (Li/Li^+). In the first cycle, the charging and discharging capacities of the composite anode are 433.5 and 289.9 mAh g^{-1}, from which its first coulombic efficiency of 66.9% is calculated. It is evident that the discharging capacity is far lower than the SbSn alloy theoretical discharge capacity of 825 mAh g^{-1}. This is probably due mainly to the presence of amorphous carbon pyrolyzed PAN. As a matter of fact, if the mass of the active material in the composite electrode was measured only by the mass of Sn–Sb alloy in the composite electrode, the first discharging capacity of

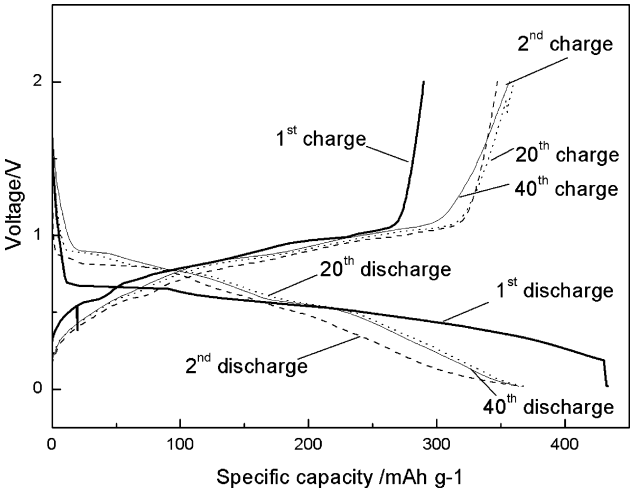

Fig. 5. The typical charge/discharge curves for the composite material at a constant current density of 0.25 mA cm^{-2} cycled between 0.02 and 2.0 V (Li/Li^+).

the composite electrode showed 722.5 mAh g^{-1}, approaching to the theoretical capacity of SnSb. According to the mass and thickness of the active electrode, 2.038 g cm^{-3} of the density of the composite anode was determined, while the pressed density of the classical graphite anode is on the order of 1 g cm^{-3}. Therefore, the density of the composite anode is approximately twice as many as that of a classical graphite anode. Moreover, low first coulombic efficiency may be related to the formation of a SEI (solid electrolyte interface) passivating film as a result of the reduction reactions of Li with electrolyte on the surface of the electrode material. Meanwhile, one should notice from the figure that the first lithiation potential plateau (0.7 V vs. Li/Li^+) is lower than that of the second as well as following one (0.8 V vs. Li/Li^+). This means that some irreversible reactions may occur during the first discharge the initial structure of Cu_2Sb and SnSb during the first discharge and additional energy is need to destroy and rearrange the initial structure of Cu_2Sb and SnSb during the first discharge.

To investigate the electrochemical behavior of composite material during charge and discharge cycles, differential capacity (dQ/dV) plots during the 1st, 2nd, 10th and 20th cycles are compared in Fig. 6. The plots show similarities in the charge processes. Nevertheless, apparent differences can be distinguished between the first two discharge processes, indicating that they follow a different reaction mechanism. We presume that the plateau voltage (0.7 V vs. Li/Li^+) on the voltage profiles corresponding to the two-phase region between Cu_2Sb and Li_3Sb, which is in good accordance with the reduction peak in the differential capacity plots. At 0.7 V, a voltage plateau signifies the onset of a two-phase reaction consistent with the formation of a $Li_{2+z}Cu_{1-z}Sb$ structure ($0 < z < 1$), closely related to Li_3Sb [18], while at 0.61 V and at lower voltages the $Li_{2+z}Cu_{1-z}Sb$ phase continues extrusion of Cu from the structure, yielding the final discharge products Li_3Sb and Cu at $z = 1$. In fact, the electrochemical profile and the differential capacity plots suggest that reaction (1) occurs by a similar inhomogeneous process of lithium insertion and copper extrusion.

$$3Li + Cu_2Sb \rightarrow Li_3Sb + 2Cu \quad (1)$$

Reaction (1) can be written more generally as:

$$2Li + Cu_2Sn \rightarrow Li_2CuSb + Cu \quad (2)$$

$$Li + Li_2CuSn \rightleftarrows Li_3Sb + Cu \quad (3)$$

Therefore, this explain the reason why there is an acute peak at 0.7 V at first discharge curve while disappearing at following discharge ones and there all are the presence of peaks at first discharge as well as following curves at 0.61 V in the differential capacity plots. Herein, note that in the same time that Cu_2Sb perform electrochemical reaction with Li, SnSb alloy does so as well and hold a dominant reaction with Li, which can be found in the charge/discharge curves and differential capacity plot of the composite material, because the composite material has the similar charge/discharge curves during electrochemical cycles except for first cycle as that of SnSb described in refs. [19,20].

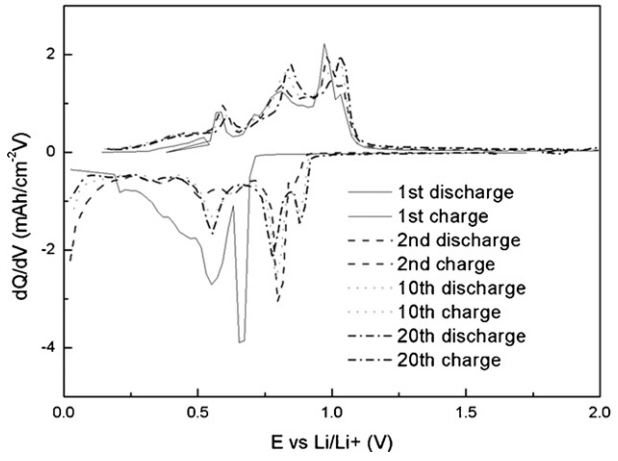

Fig. 6. The differential capacity (dQ/dV) plots of the composite material during the 1st, 2nd, 10th and 20th cycles.

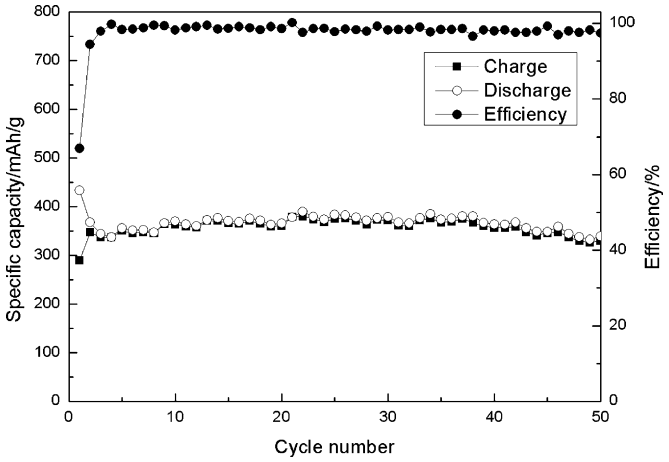

Fig. 7. The cycle performance and coulombic efficiencies of the composite material.

Fig. 7 shows the cycle performance and coulombic efficiencies of the composite material. The reversible capacity was 339.5 mAh g^{-1} after 50 cycles, corresponding to 78.6% of the discharge capacity retention. Except for lower first charge/discharge efficiency, charge/discharge efficiencies of following cycles keep higher values and 50th cycle efficiency still reached 97.4%. It is considered that good cycle performance of the composite material can be attributed to two factors. First, amorphous carbon membrane formed by pyrolysis of PAN in the composite material serves as a supporting medium, which would both buffer the volume expansion of Sn–Sb alloy and prohibit the aggregation of Sn or Sb micro-particles and maintain the conduction path between Sn or Sb particles and amorphous carbon. Second, electrodeposited Sn–Sb alloy phase presented isolated pillar-like structure, which would reduce the mechanical stress resulting from phase transition structure and restricted volume expansion during Li insertion and extraction processes.

4. Conclusion

Applying a phase inversion process to make PAN solution containing PEG cast on a Cu foil turn into microporous membrane coated on the Cu foil, and using the microporous membrane electrode as a template-like, a composite material anode for LIB can be successfully prepared through electrodepositing Sn–Sb alloy on the template-like electrode via the membrane pores and then heat-treatment. This composite electrode has a novel structure that most of Sn–Sb alloy are dispersed in isolated pillar-like structure electrodeposited on Cu current collector in a conductive microporous carbon membrane except that some excess Sb form Cu_2Sb alloy with Cu which diffuses from Cu current collector. In here, the micro-porous carbon membrane deriving from low temperature pyrolysis of PAN serves as supporting medium, which relaxes the problematic volume change of SnSb alloy during intercalation/de-intercalation Li^+ and inhibits aggregation of some dispersive SnSb or Cu_2Sb micro-particle. Electrochemical test results showed that the composite electrode exhibited desirable cycle performance and acceptable cycling coulombic efficiencies. We believe that it is a

promising method to use the supporting medium idea in the process of preparing anode material for LIB.

References

[1] K.D. Kepler, J.T. Vaughey, M.M. Thackeray, J. Power Sources 82 (1999) 383.
[2] J.O. Besenhard, J. Yang, M. Winter, J. Power Sources 68 (1997) 87.
[3] H.P. Zhao, X.M. He, C.Y. Jiang, C.R. Wan, Prog. Chem. 18 (2006) 1710.
[4] W.H. Pu, X.M. He, J.G. Ren, C.R. Wan, C.Y. Jiang, Electrochim. Acta 50 (2005) 4140.
[5] J. Yang, M. Winter, J.O. Besenhard, Solid State Ionics 90 (1996) 281.
[6] D.G. Kim, H. Kim, H.J. Sohn, T. Kang, J. Power Sources 104 (2002) 221.
[7] J.G. Ren, X.M. He, C.Y. Jiang, C.R. Wan, Acta Metall. Sin. 42 (2006) 727.
[8] H.W. Yan, S. Sokolov, J.C. Lytle, A. Stein, F. Zhang, W.H. Smyrl, J. Electrochem. Soc. 150 (2003) A1102.
[9] S.D. Beattie, J.R. Dahn, J. Electrochem. Soc. 150 (2003) A894.
[10] J.G. Ren, W.H. Pu, X.M. He, C.R. Wan, C.Y. Jiang, J. Mater. Sci. Technol. 21 (2005) 770.
[11] K. Wang, X.M. He, L. Wang, J.G. Ren, C.Y. Jiang, C.R. Wan, J. Electrochem. Soc. 153 (2006) A1859.
[12] J.G. Ren, X.M. He, W.H. Pu, C.Y. Jiang, C.R. Wan, Electrochim. Acta 52 (2006) 1538.
[13] K. Wang, X.M. He, J.G. Ren, C.Y. Jiang, C.R. Wan, Electrochem. Solid State Lett. 9 (2006) A320.
[14] H.P. Zhao, C.Y. Jiang, X.M. He, C.R. Wan, Acta Metall. Sin. 43 (2007) 775.
[15] X.M. He, W.H. Pu, L. Wang, J.G. Ren, C.Y. Jiang, C.R. Wan, Electrochim. Acta 52 (2007) 3651.
[16] L.B. Wang, S. Kitamura, T. Sonoda, K. Obata, S. Tanase, T. Sakai, J. Electrochem. Soc. 150 (2003) A1346.
[17] N. Tamura, R. Ohshita, M. Fujimoto, S. Fujitani, M. Kamino, I. Yonezu, J. Power Sources 107 (2002) 48.
[18] L.M.L. Fransson, J.T. Vaughey, R. Benedek, K. Edstrom, J.O. Thomas, M.M. Thackeray, Electrochem. Commun. 3 (2001) 317.
[19] C.L. Yin, H.L. Zhao, H. Guo, X.L. Huang, W.H. Qiu, J. Univ. Sci. Technol. Beijing 14 (2007) 345.
[20] Y. Chaoli, Z. Hailei, G. Hong, Q. Weihua, J. Xidi, Rare Met. Mater. Eng. 36 (2007) 1403.